JOURNAL OF COMPUTATIONAL PHYSICS **125,** 488–497 (1996)
ARTICLE NO. 0110

Numerical Modeling of Space-Charge-Limited Charged-Particle Emission on a Conformal Triangular Mesh

STANLEY HUMPHRIES JR.

Department of Electrical and Computer Engineering, University of New Mexico, Albuquerque, New Mexico 87131

Received June 9, 1995; revised October 16, 1995

Orbit tracing is a numerical technique to design high-current charged particle guns and transport systems. Although most available programs use the finite-difference approach to calculate electric fields, the finite-element method has advantages for accuracy and versatility. This paper describes an effective algorithm to model space-charge-limited emission and a procedure to apply it to variable-resolution conformal triangular meshes with multiple emission regions. Improved tabulations of space-charge solutions for sharply curved emission surfaces are given. In a benchmark Pierce diode simulation, the procedure gives an absolute current prediction within 0.2% of the analytic value and particle orbits within 0.1° of the predicted exit angle. © 1996 Academic Press, Inc.

1. INTRODUCTION

High-current electron guns are used in microwave sources, beam welders, materials processing accelerators, and a range of other applications [1]. Beam-generated electric fields strongly influence the characteristics of these devices, and numerical calculations are essential for their design. In most applications, the beam pulse length is much longer than the electron transit time. In this regime, orbit tracing codes [2] are effective tools to find self-consistent electric fields and beam current density. Several computer programs exist for electron and ion gun design [3–7]. With the exception of the Demeos code [7], they use finite-difference methods on square or rectangular meshes to solve the Poisson equation. This paper describes the technique to model space-charge emission in the finite-element Trak code [8]. The method can accommodate multiple emission regions with arbitrary source shapes and triangular mesh geometries. Section 2 reviews orbit tracing and finite-element field solutions. The discussion concentrates on two-dimensional geometries, including the important cases of cylindrically symmetric guns and slot injectors. The section also describes the assignment of space-charge to a finite-element mesh from model particle traces. Section 3 summarizes a method to calculate particle orbits near an emission surface. The method gives an accurate representation of local space-charge and avoids the numerical problem of zero-velocity particles. A one-dimensional model confirms the approach and yields information on accuracy and strategies to ensure convergence. Section 4 discusses application of the method on a two-dimensional finite-element mesh. Section 5 summarizes correction factors to improve the accuracy of space-charge-limited emission calculations from curved electrodes. The method makes it easy to model curved and planar sources with mixed source-limited and space-charge-limited flow.

2. BEAM-GENERATED FIELDS ON A FINITE-ELEMENT MESH

Figure 1 shows a conformal mesh near an electron-emitting surface. The mesh divides the vacuum space into triangular elements that closely match the boundary surfaces. The size of the triangles can be adjusted to give fine resolution in regions of strong field variations. The finite-element expression of the Poisson equation proceeds from the integral form of the Maxwell equations applied over the triangles that surround each mesh vertex [9–11]. In the linear approximation, volume quantities like space-charge and dielectric permeability are constant over each triangle. The numerical form of the Poisson equation relates the potential at each vertex to the potentials at the neighboring points and the characteristics of the six surrounding triangles. The following discussions assume a regular mesh with six triangles of area a_i adjacent to each point. Figure 2 defines the mesh geometry near a test point. The numerical equivalent of the Poisson equation is

$$\Phi_o = \frac{\sum_{i=1}^{6} W_i \Phi_i + \sum_{i=1}^{6} \rho_i a_i}{\sum_{i=1}^{6} W_i}, \tag{1}$$

Equation (1) states that the vertex potential is a weighted average of the potential values at the nearest neighbors and the surrounding space-charge. The weighting factors are given by

0021-9991/96 $18.00

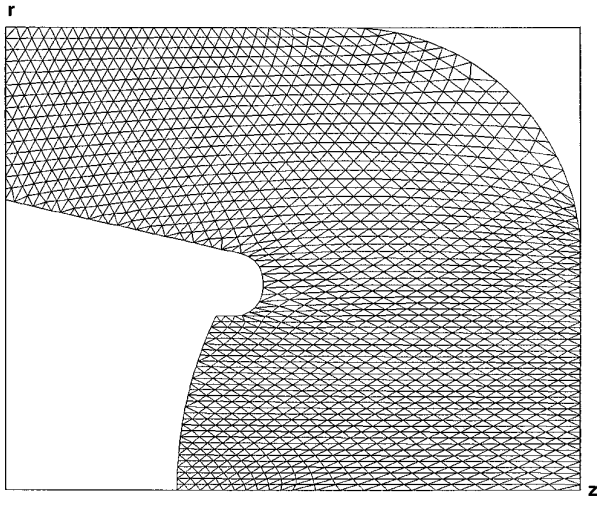

FIG. 1. Example of a conformal triangular mesh with variable resolution matched to electrode surfaces.

$$W_1 = \frac{\varepsilon_1 \cot(\theta_{1a}) + \varepsilon_2 \cot(\theta_{2b})}{2}$$

...

$$W_6 = \frac{\varepsilon_6 \cot(\theta_{6a}) + \varepsilon_1 \cot(\theta_{1b})}{2}.$$

Figure 2 defines the angles that characterize the triangle geometries. Equation (1) represents a large set of coupled linear equations. These equations can be solved by iterative relaxation or by a direct solution using matrix algebra [9].

Space-charge arises from the beam density in charged-particle gun calculations. The standard technique to estimate $\rho(\mathbf{x})$ is to represent a beam with a moderate number of model particles [2]. Because of the laminar behavior of particle distributions under the Vlasov equation, a model particle can represent the average behavior of many nearby particles in phase space. The procedure is to follow the orbits of model particles in the total electric and magnetic fields as if they were single electrons (or ions), but to assign space-charge along the trajectory as though the model particle carried the charge of many adjacent particles. The procedure to assign space-charge to mesh triangles is straightforward. A Runge–Kutta integration [12] of the equations of the motion with time step Δt yields a set of closely spaced coordinates $\mathbf{x}(n\,\Delta t)$ and the positions at intermediate time steps, $\mathbf{x}([n + \frac{1}{2}]\,\mathbf{\Delta} t)$. The indices of the triangle occupied by the particle at the intermediate time are available from the electric field calculation. Over a time step in the orbit solution for particle j, the space-charge density of the triangle is incremented by

$$\Delta\rho = \frac{I_j\,\Delta t}{\Delta V}. \tag{2}$$

In Eq. (2), I_j is the current for model particle j and ΔV is the volume represented by the triangular. For example, in cylindrical coordinates the volume is $\Delta V = 2\pi r_a\,\Delta A$, where ΔA is the triangle area and r_a is the radius of the triangle centroid.

The challenge to finding self-consistent electric fields is that the particle orbits are not known in advance; therefore, the quantity $\rho(\mathbf{x})$ and the fields are unknown. The resolution in orbit tracing programs is to use an iterative approach. Initially, the total fields are set equal to the applied field and a set of model particle trajectories are calculated. Space-charge deposition follows the prescription of Eq. (2). The fields are then recalculated with the addition of $\rho(\mathbf{x})$. The corrected fields give modified particle orbits that, in turn, lead to an improved field calculation. With appropriate charge averaging, the process converges to the correct self-consistent fields, even for high-intensity beams.

The calculation is more difficult for beams from a space-charge limited source [13]. Here, the model particle currents are not known in advance—they depend on the electric field intensity near the source. The problem is that space-charge-limited emission coincides with zero electric field at the source surface. In a numerical model, it is impossible to start model particles at this surface because they will not advance. The solution is to create the particles at a hypothetical emission surface and to determine the model particle current from a local application of analytic formulae. Sections 3 and 4 describe the method used in Trak. In contrast to other ray tracing codes, the method

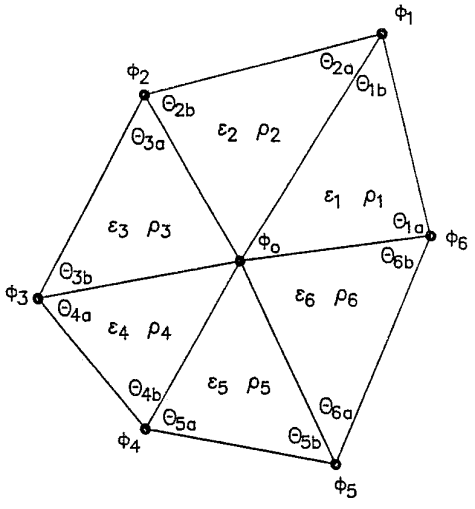

FIG. 2. A point of a finite-element triangular mesh—six neighboring mesh points define six surrounding triangles. Definitions of quantities for linear approximation of the Poisson equation.

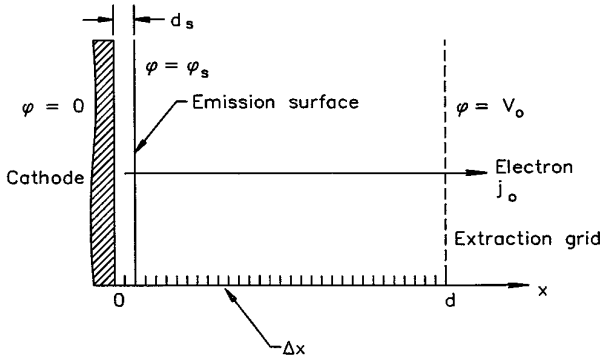

FIG. 3. One-dimensional acceleration gap for electrons. Definition of quantities for the Child law solution and numerical calculation of space-charge-limited emission.

is compatible with arbitrary mesh and source geometries and multiple regions of emission.

3. ONE-DIMENSIONAL MODEL FOR SPACE-CHARGE-LIMITED EMISSION

This section reviews the numerical calculation of space-charge-limited emission in the one-dimensional gap of Fig. 3—results can be checked against Child law [14] predictions. The discussion holds for electrons—it can be easily extended to ions. The gap has width d and an applied voltage of $+V_o$. The condition of space-charge-limited flow is that the electron density approaches a value that reduces the electric field on the cathode surface to zero. For nonrelativistic electrons, the Poisson equation for electrostatic potential is

$$\frac{d^2\phi}{dx^2} = \frac{j_o}{\varepsilon_o\sqrt{2e\phi/m_e}}. \tag{3}$$

In Eq. (3), the quantity j_o is the current density, a constant over the gap. The solution of the equation with the following boundary conditions determines the value of j_o: $\phi(0) = 0$, $d\phi(0)/dx = 0$, and $\phi(d) = V_o$. Equation (3) can also be written in terms of the dimensionless variables $\Phi = \phi/V_o$ and $\chi = x/d$ as

$$\frac{d^2\Phi}{d\chi^2} = \frac{\Gamma}{\sqrt{\Phi}}, \tag{4}$$

where

$$\Gamma = \frac{j_o d^2}{\varepsilon_o\sqrt{2e/m_e}}\, V_o^{3/2}. \tag{5}$$

The solution of Eq. (4) with $\Phi(0) = 0$, $\Phi'(0) = 0$, and $\Phi(1) = 1$ gives $\Gamma = 4/9 = 0.444444$, equivalent to

$$j_o = \left(\frac{4\varepsilon_o}{9}\right)\sqrt{\frac{2e}{m_e}}\,\frac{V_o^{3/2}}{d^2}. \tag{6}$$

Equation (6) is the familiar Child law [14]. The electrostatic potential varies as

$$\phi = V_o(x/d)^{4/3}.$$

The electric field is zero at $x = 0.0$ and has the value

$$E_x = -(4/3)\ V_o/d \tag{7}$$

at $x = d$.

To find a numerical solution for space-charge flow, we apply the Child law over an emission surface at the cathode of width d_s. The surface is much thinner than the gap, $d_s \ll d$. The potential of the emission surface relative to the source is $\phi_s(d_s)$. Nonrelativistic expressions are valid if d_s is small enough so that $e\phi_s \ll m_e c^2$. At the surface electrons have the velocity

$$v_e = [2e\phi_s/m_e]^{1/2}. \tag{8}$$

Electrons always have nonzero velocity in the region to the right of the emission surface; therefore, the associated space-charge follows from an integration of the relativistic equations of motion and the prescription of Eq. (2). Problems arise assigning space-charge to mesh elements to the left of the emission surface. Direct calculations from the analytic Child law expressions are difficult to extend to a two-dimensional triangular mesh. Writing a program that can reliably perform volume integrations for arbitrary mesh and emitter surface geometries is challenging. An alternative is to project model electrons backward to the source from the emission surface with the velocity magnitude of Eq. (8), assigning space-charge according to Eq. (2). This procedure can lead to density divergences for solutions near the space-charge limit when the model particle velocity approaches zero.

The Trak program uses a variant of the second method that avoids the problem of density divergence. To illustrate the method, consider the one-dimensional model of Fig. 3. The goal is to find a numerical solution of the Poisson equation by tracking a single model particle from the emission surface. The calculation is initialized with the applied field solution, a uniform electric field $E_x = -V_o/d$. The initial potential at the emission surface is

$$\phi_s = V_o(d_s/d).$$

The model particle carries the current $I = jA$, where

$$j = \left(\frac{4\varepsilon_o}{9}\right)\sqrt{2e/m_e}\,\frac{\phi_s^{3/2}}{d_s^2} \tag{9}$$

and A is a unit area. To find the charge density to the right of the surface, the model electron is created at the emission surface with velocity

$$v_x = (2e\phi_s/m_e)^{1/2} \tag{10}$$

and advanced with uniform time step Δt. The problem is how to assign charge to the left of the emission surface while avoiding a zero velocity model particle. One solution is to take a uniform density that gives the same value of electric field at the emission surface as the Child law, Eq. (7). This method has the advantage that a uniform density can be impressed on a two-dimensional triangular mesh simply by projecting constant-velocity model particles backwards. This circumvents dealing with the complexities of mesh and emission surface geometries. Inspection of the solution of the one-dimensional Poisson equation gives the desired density value $\rho_o = 4\varepsilon_o\phi_s/6d_s^2$. This density results if the model particle moves backward from the emission surface to the source with the current density of Eq. (9) and with a constant velocity equal to two-thirds that of Eq. (10),

$$v_x = -(\tfrac{2}{3})\sqrt{2e\phi_s/m_e}.$$

This method is easy to implement on a two-dimensional mesh because the logic of particle charge assignment and tracking is almost identical for the forward and backward orbit integrations. The only difference is to set electric field values equal to zero during the backward trace. After several iterations, the emission surface potential approaches

$$\phi_s = V_o(d_s/d)^{4/3},$$

and the model particle current density, I/A, approaches the value of Eq. (6).

One-dimensional finite-element calculations were made to test the procedure and to document parameter sensitivities. The model used a uniform element size of Δx. Back-substitution [15] was applied to solve the one-dimensional Poisson equation, and particle orbits were advanced with a second-order Runge–Kutta routine. The free parameters in the model were NMesh (the number of elements across the gap), d_s/d (the relative distance of the emission surface from the source), and Δt (the time step for the orbit integration). The scaling parameter for the time step was the transit time across a cell for a particle moving at the exit velocity,

$$\Delta t_o = \frac{\Delta x}{\sqrt{2eV_o/m_e}}.$$

To achieve stable convergence over the range of parameter choices, it was necessary to introduce two correction factors. The first was a suppression factor, applied on initial iteration cycles. On the first cycle, the applied electric field at the emission surface was much larger than the final self-consistent value. Therefore, application of Eq. (9) gives excessive space-charge. This often caused an instability between cycles—the emission current was alternately enhanced and depressed near the cathode. One improvement was to use a gentle start, multiplying the value of Eq. (9) by a graded sequence of numbers less than unity during initial cycles. In addition, charge averaging between iteration cycles also reduced emission instabilities. Instead of zeroing the values of ρ_k for each particle tracking cycle, they were initially set equal to a fraction of the space charge from the previous cycle.

$$\rho_k^n = (1-\varepsilon)\rho_k^{n-1}.$$

Here, ε is a number between 0.0 and 1.0. During particle tracking, the incremental space-charge is

$$\rho_k^n = \rho_k^n + \varepsilon\,\Delta\rho_k.$$

A value of $\varepsilon = 1.0$ corresponds to no averaging. A value $\varepsilon \ll 1$ gives averaging over several previous cycles. On the first cycle, ε is set equal to 1.0. Generally, a value of $\varepsilon = 0.5$ gave stable one-dimensional calculations. A low value is essential for two-dimensional calculations with complex reflex orbits.

Runs were made to check the effect of the mesh size, given by the parameter NMesh, on the solution accuracy. The emission region occupied 10% of the gap, the space charge averaging factor was $\varepsilon = 0.5$ and the time step was short. The calculations converged in about 15 cycles. The tabulated error is the difference between the predicted current density and the Child law value. The error dropped to 0.34% with only 20 mesh boxes. A second test checked the effect of the emission region width, d_s/d. These runs used NMesh = 50 and a short time step. The accuracy was 0.07% for $d_s/d = 0.08$ and had the acceptable value of 0.43% for an emission extending over only one mesh element. It is noteworthy that the method converges to the correct value of current density, even when the emission region fills the entire gap. In the one-dimensional model, the current density was almost independent of d_s/d. Nonetheless, it is important to note that two-dimensional calculations require that $d_s/d \ll 1$. In this limit the surface conforms to the source shape and the errors in the transverse electric

field resulting from the assumption of uniform density are correspondingly small.

The final test checked the effect the time step size for NMesh = 50 and $d_s/d = 0.10$. For a value $\Delta t/\Delta t_o \ll 1$, the model particle took several time steps to cross each mesh element, giving a smooth distribution of $\rho(x)$. For the value $\Delta t/\Delta t_o = 20.0$, the paricle crossed many mesh elements in a time step giving an irregular distribution of space-charge. Even for this extreme case the method converged to a current density value within 0.3% of the Child law value. In summary, the one-dimensional tests confirm that the constant density procedure gives good accuracy for $\Delta x < d/20$, an emission distance of about 0.10 of the acceleration gap and a value of Δt such that particles travel about one mesh unit per time step near the emission surface. In two-dimensional calculations, these conditions can be easily satisfied on a variable resolution triangular mesh.

4. PROCEDURES FOR SPACE-CHARGE-LIMITED EMISSION IN TWO DIMENSIONS

The space-charge emission method of Section 3 can be applied to two-dimensional calculations on a finite-element triangular mesh. The main tasks are to identify source points, to set emission surface points, and to assign effective areas to model particles. The first step is to set emission surfaces on the electrodes. This task is accomplished during mesh generation by assigning a special flag to surface points that emit particles. For space-charge deposition, there is little advantage to choosing the spacing between particles smaller than the local mesh triangle size. Therefore, the convention in the Trak program is to create a model particle at each of the emitting source points. The mesh resolution at the source determines the number of model particles in the beam. The Trak program handles up to 10 separated emission surfaces. The term *set* denotes the surface points and model particles that constitute an individual emission surface.

After reading the computational mesh, the initial task of the tracking program is to collect the source points in each set and to arrange them spatially in order of distance from a reference point. The user can specify reference points for each set to resolve ordering ambiguities. With judicious choices of reference points and sets, Trak can model emission from any shaped surface, including indentations and discontinuities. Figure 4 illustrates the definition of surface points, sets, and reference points. The figure also shows point ordering. The next task is to compute the distance span of each model particle on the source surface, $D_s(i)$, where i is the model particle index. These quantities are used to find the effective cross-section areas of the model particles. For the inside particles of a set, $D_s(i)$ equals the distance between points halfway to the adjacent particles (Fig. 4). For the two outside particles of a set,

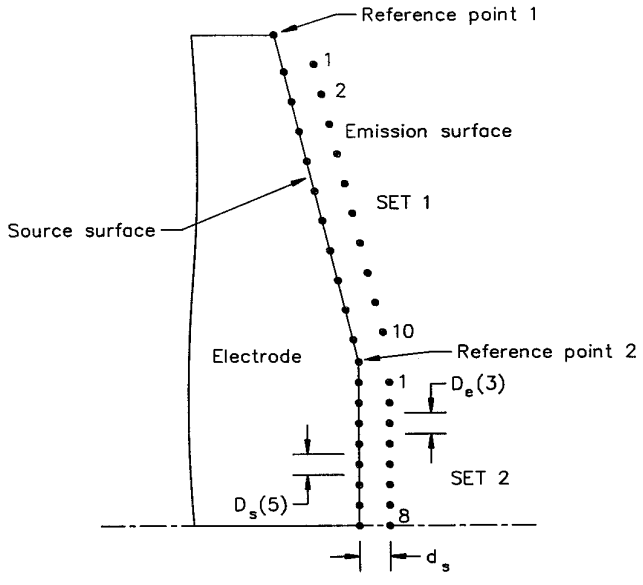

FIG. 4. Definition of two emission regions on a shaped cathode, showing two sets of ordered source points, projected emission surface points, and distance spans at the source and emission surfaces.

there are two options to set the spans. For a sharp emission edge, the quantity $D_s(i)$ equals the distance from the edge point halfway to the adjacent point. This convention gives correct total current if the end points represent the edge of the source. The second option is applied to blend the current density from two or more adjacent sets. In this case, the distance span equals the full distance to the adjacent particle of the set.

The third task of the particle tracking program is to determine a set of points at a distance d_s from the source that constitutes the emission surface. Trak performs this operation geometrically. For each inside point of a set, the program finds a unit vector normal to the local source surface using the positions of the two adjacent points. The vector is then used to compute the corresponding emission surface point (Fig. 4). For the end points of a set, the vector calculation uses the coordinates of the end point and one adjacent point. In general, sources may be concave or convex—the surface point locations alone do not fully constrain the normal vector. The procedure in Trak is to move in one direction and then to make a sample electric field calculation. If the procedure returns an error, the point is inside an electrode or outside the computational region. In this case, the program tries the opposite direction. This procedure gives the correct emission surface location for any source shape or orientation—it also signals an error for source concavities that are too small to enclose the emission surface. Once a set of consistent surface points is known, Trak computes the emission surface distance spans, $D_e(i)$, using the same conventions applied to the source points. These quantities give the effective model

particle areas at the emission surface, $A_e(i)$. For example, the expression in cylindrical coordinates is

$$A_e(i) = 2\pi r_i D_e(i),$$

where r_i is the distance from the emission point to the z-axis.

At this point, the program has enough information to apply the space-charge procedure of Section 3. On each tracking cycle, Trak first calculates values of the electric field and the potential difference from the source, ϕ_s, at every emission point. For flat or mildly curved surfaces, substituting the quantities ϕ_s and d_s in Eq. (9) gives a good approximation to the emission surface current density. (Section 5 derives corrections for highly curved surfaces.) The total current of a model particle is the product of the current density and $A_e(i)$. The program assigns each electron a constant velocity $\frac{2}{3}(2e\phi_s/m_e)^{1/2}$ aligned parallel to the local electric field and tracks it backward to the source, assigning space-charge according to Eq. (9). Next, the program gives each electron an initial velocity with magnitude $(2e\phi_s/m_e)^{1/2}$ aligned anti-parallel to the electric field and advances it by the relativistic equations of motion, assigning a charge along the way. Trak includes a variety of particle orbit termination options—a model particle may stop if it enters an electrode or dielectric, leaves the solution region, exceeds a maximum time, or crosses a special interpolation plane. After all the model electron trajectories are complete, the program updates the electrostatic potential using Eq. (1). The process repeats for several cycles until the solution converges. The two-dimensional calculations use the gentle-start suppression factors and charge averaging procedures discussed in Section 3.

To demonstrate the accuracy of the methods in a two-dimensional calculation, consider the standard Pierce diode for a sheet electron beam [16]. Figure 5a illustrates the geometry. The system extends out of the page and has reflection symmetry about the bottom axis. The flat surface on the left is a proton emitter. The focusing electrode above the emitter inclines at an angle of 22.5°. This electrode, combined with the shaped cathode and extraction grid on the right, ensures uniform current density over the source surface and parallel orbits for the exiting protons. Equation (6) gives the current density with d equal to the distance between the emitter and the extraction grid and with V_o equal to the anode–cathode voltage. In this example, values of $d = 2.0$ cm and $V_o = 50$ kV give a predicted current density of 0.1528 A/cm^2. The Trak calculation uses the 4500 point mesh of Fig. 5b with variable resolution. Note the resolution enhancements in the propagation and emission regions. The calculation takes 135 s for 20 tracking cycles on a 90 MHZ Pentium [17] computer. With an emission surface distance of $d_s = 2$ mm, the code prediction of current density is 0.1530 A/cm^2. This figure is within 0.2% of the analytic value. Figure 5c shows the orbits of 61 model particles and equipotential lines for the self-consistent field. As expected, the equipotential lines are normal to the beam boundary, and the proton orbits are parallel to within ±0.1° at the extraction grid. The current density at the emission surface is uniform to within +0.2%. The accuracy is similar to that reported for the Demeos code [7]. A comparison calculation was made with Egun [3], a finite difference code that uses a uniform square mesh. The calculation used 3200 mesh points, 20 tracking cycles, 82 model particles, and the same emission surface distance. The total current prediction was in error by about 1%. In the final solution, there was a systematic variation of current density and particle divergence from the axis to the beam outer edge. The current density varied by about 5% and there was an 0.75° beam divergence at the edge.

5. CORRECTIONS FOR SHARPLY CURVED ELECTRODES

The application of Eq. (9) to calculate emission surface current density is adequate for many conventional electron and ion guns, but corrections are necessary for the accurate representation of emission from sharply curved surfaces. Initially, we shall concentrate on solutions in rectangular coordinates. Here, surfaces vary in x and y but extend a long distance in z. Figure 6 illustrates a blade emitter. The standard planar Child law (Eq. (9)) applies to the flat regions where $D_e(i) \cong D_s(i)$. Corrections are necessary at the sharply curved edges, where $D_e(i) > D_s(i)$. Correction factors can be estimated by assuming that flow in the section of the emission region corresponding to a model particle approximates space-charge-limited flow in a cylindrical section. Numerical solutions in cylindrical and spherical coordinates have long been available. A familiar example is the Langmuir α function for spherical flow [18]. Nonetheless, it is worthwhile to extend the calculations to determine high-accuracy correction factors that are better suited to particle tracking codes.

The insert of Fig. 6 illustrates the geometry for diverging flow. If the angular span of an edge section is much smaller than 1 radian, then the distance spans are related to the inner and outer radii of the equivalent cylindrical solution by

$$\frac{D_e(i)}{D_s(i)} \cong \frac{r_o}{r_i}.$$

Given an emission surface spacing

$$d_s = r_o - r_i, \tag{11}$$

and a potential difference of ϕ_s, the goal is to find the

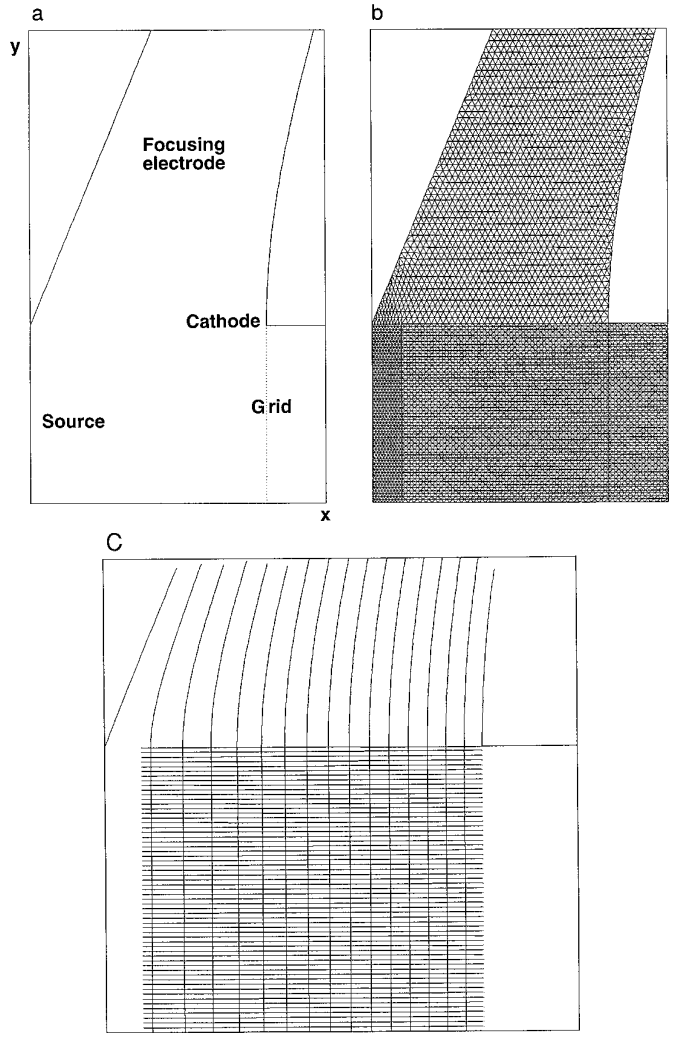

FIG. 5. Benchmark test of the ideal Pierce diode—structure extends out of page and is symmetric about the bottom axis: (a) Geometry and electrode potentials ($x_{\min}$, 0.0 cm; $x_{\max}$, 2.5 cm; $y_{\min}$, 0.0 cm; $y_{\max}$, 4.0 cm). (b) Variable resolution mesh used for a TRAK simulation. (c) Detailed view of model particle orbits and equipotential lines for the self-consistent field solution ($x_{\min}$, 0.0 cm; $x_{\max}$, 2.5 cm; $y_{\min}$, 0.0 cm; $y_{\max}$, 2.5 cm).

current density at the outer radius (emission surface). It is convenient to compare the solution to the prediction of Eq. (9) for the same values d_s and ϕ_s to define a curvature correction factor, F_c. This number is a function of the ratio of distance spans,

$$\beta_i = D_e(i)/D_s(i).$$

The values of β_i are easily calculated for each model particle during the emission surface setup procedure. Correction of the current density simply involves multiplying the current density at each emission point determined from Eq. (9) by $F_c(\beta_i)$.

Consider the diverging flow of electrons in the cylindrical region of Fig. 6. The electrons move from r_i at ground potential to r_o at $\phi = V_o$, where the difference between the radii equals d_s (Eq. (11)). If j_o is the current density at the emission surface, then the electron space-charge density is given by

$$\rho(r) = -j_o r_o / r v_r.$$

Taking the radial velocity as

$$v_r = (2e\phi/m_e)^{1/2},$$

the Poisson equation is

$$\frac{1}{r}\frac{d}{dr} r \frac{d\phi}{dr} = \frac{j_o r_o}{\varepsilon_o r \sqrt{2e\phi/m_e}}.$$

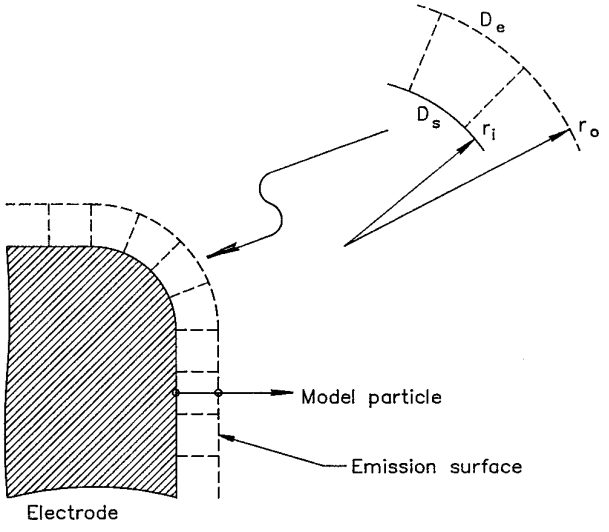

FIG. 6. Cylindrical correction for elements on the curved surface of a blade emitter—structure extends out of page.

Introducing the dimensionless variables $\Phi = \phi/V_o$ and $R = r/d_s$, we can rewrite the above equation as

$$\frac{1}{R}\frac{d}{dR}R\frac{d\Phi}{dR} = \frac{\Gamma R_o}{\sqrt{\Phi}}, \tag{12}$$

where $R_o = r_o/d_s$ and Γ is given by Eq. (5).

Equation (12) holds over the range $R_i = r_i/d_s < R < R_o$ and satisfies following boundary conditions

$$\begin{aligned} \Phi(R_i) &= 0.0, \\ d\Phi(R_i)/dR &= 0.0, \end{aligned} \tag{13}$$

and

$$\Phi(R_o) = 1.0.$$

The inner and outer radii can be written in terms of β as

$$\begin{aligned} R_i &= 1/(\beta - 1), \\ R_o &= \beta/(\beta - 1). \end{aligned} \tag{14}$$

Solution of the boundary value problem gives a value of Γ that in turn determines the space-charge-limited current density, j_o. The curvature adjustment factor is related to the value of Γ by

$$F_c(\beta) = 9\Gamma(\beta)/4.$$

Equation (12) was solved with a fourth-order Runge–Kutta integration. The integration started at R_o with approximate initial values of Γ and $d\Phi(R_o)/dR$. A shooting calculation [19] located values of the parameters for which the equation satisfied the boundary conditions at R_i (Eqs. (13)). Using the planar Poisson equation as a test, the number of iterations and the variational parameters were adjusted for accuracy to five decimal places. The solution was almost the same for convergent beams—the only change was to take the initial radii as

$$\begin{aligned} R_i &= 1/(1 - \beta), \\ R_o &= \beta/(1 - \beta). \end{aligned} \tag{15}$$

Table I shows the current adjustment factor with accuracy to four decimal places calculated from 100 shooting cycles. The table encompasses the full practical range. For larger or smaller values of β, the potential variation near the surface is poorly represented by the assumption of a cylindrical section. The following series expansion gives F_c accurate to 5×10^{-4} over the range of the table:

$$F_c = 0.7860 + 0.2282/\beta - 0.0142/\beta^2.$$

Curvature corrections for systems with cylindrical symmetry are more involved. If the emitter surface has a center of curvature on the z-axis, then space-charge flow in an element is spherical. This case corresponds to the element marked *a* in Fig. 7. The spherical Poisson equation has the form

$$\frac{1}{R^2}\frac{d}{dR}R^2\frac{d\Phi}{dR} = \frac{\Gamma R_o^2}{\sqrt{\Phi}}.$$

The above equation has the same boundary conditions as Eq. (12). Equations (14) and (15) relate the inner and outer dimensionless radii to the parameter $\beta = D_e/D_s$ for diverging and converging flows. Solution of the above equation gives the spherical correction factor, $F_c(b)$, listed in Table I. The spherical correction factor is related to the Langmuir function [18] by

$$F_c = 1/\alpha R_o^2.$$

The quantity F_c is better suited to tabulation and series approximation because it is close to unity over the range of the table, while the Langmuir function varies over several orders of magnitude. The following expansion gives a good approximation to the values of Table I:

$$\begin{aligned} F_c = 0.4281 + 0.8060/\beta - 0.3094/\beta^2 \\ + 0.0845/\beta^3 - 0.0092/\beta^4. \end{aligned}$$

Spherical corrections do not apply in cylindrical coordinates to cases where the center of curvature of a surface

TABLE I

Curvature Adjustment Factor

(Converging beams)		
β	Fc Cylinder	Fc Sphere
0.300	1.3915	1.6699
0.325	1.3537	1.6114
0.350	1.3207	1.5592
0.375	1.2914	1.5124
0.400	1.2653	1.4701
0.425	1.2417	1.4316
0.450	1.2205	1.3965
0.475	1.2012	1.3641
0.500	1.1834	1.3344
0.525	1.1672	1.3067
0.550	1.1523	1.2811
0.575	1.1386	1.2570
0.600	1.1258	1.2345
0.625	1.1139	1.2135
0.650	1.1028	1.1935
0.675	1.0925	1.1748
0.700	1.0828	1.1573
0.725	1.0736	1.1404
0.750	1.0650	1.1247
0.775	1.0569	1.1096
0.800	1.0493	1.0952
0.825	1.0421	1.0815
0.850	1.0351	1.0682
0.875	1.0286	1.0558
0.900	1.0225	1.0437
0.925	1.0164	1.0322
0.950	1.0108	1.0212
0.975	1.0056	1.0106
1.000	1.0000	1.0000

(Diverging Beams)		
β	Fc Cylinder	Fc Sphere
1.050	0.9908	0.9811
1.100	0.9820	0.9631
1.150	0.9739	0.9464
1.200	0.9665	0.9307
1.250	0.9595	0.9161
1.300	0.9532	0.9021
1.350	0.9471	0.8891
1.400	0.9415	0.8767
1.450	0.9363	0.8650
1.500	0.9314	0.8540
1.550	0.9269	0.8434
1.600	0.9226	0.8333
1.650	0.9185	0.8238
1.700	0.9147	0.8146
1.750	0.9109	0.8058
1.800	0.9075	0.7975
1.850	0.9044	0.7894
1.900	0.9012	0.7815
1.950	0.8983	0.7741
2.000	0.8956	0.7671
2.050	0.8929	0.7601
2.100	0.8904	0.7536
2.150	0.8879	0.7471
2.200	0.8857	0.7410
2.250	0.8834	0.7349
2.300	0.8814	0.7291
2.350	0.8794	0.7237
2.400	0.8776	0.7183
2.450	0.8758	0.7129
2.500	0.8740	0.7079
2.550	0.8722	0.7030
2.600	0.8706	0.6980
2.650	0.8690	0.6935
2.700	0.8677	0.6890
2.750	0.8661	0.6845
2.800	0.8648	0.6802
2.850	0.8634	0.6760
2.900	0.8623	0.6719
2.950	0.8609	0.6681
3.000	0.8598	0.6643

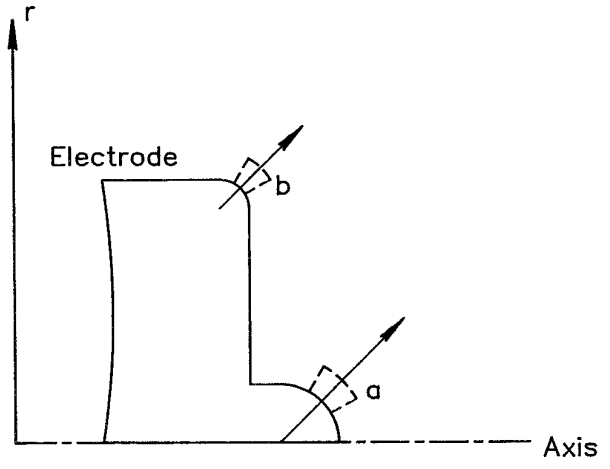

FIG. 7. Cylindrical emitter—a figure of revolution about the axis. A spherical correction is applied to surface element *a* and a cylindrical correction to element *b*.

element does not lie on the z-axis. For example, the element marked b in Fig. 7 is a sharp radius on the outside of a cylindrical emitter. The radial displacement of the element at the emission surface is almost the same as at the source. Here, it is more accurate to apply cylindrical corrections. The convention of Trak is to apply cylindrical corrections to all elements by default—spherical corrections are applied to a set only if requested by the user.

It is easy to model guns with mixed source and space-charge limited emission. Suppose there is a limit j_s on the current density at the source surface. For model particles on each tracking cycle, Trak computes the predicted current density at the emission surface from the equation

$$j_e = -\frac{4\varepsilon_o}{9}\sqrt{2e/m_e}\,\frac{\phi_s^{3/2}}{d_s^2}\,F_c(\beta_i).$$

In cylindrical coordinates, the emission surface current density projected to the source is $j_e\beta_i$. If $j_e\beta_i < j_s$, the emission current density is set equal to j_i; otherwise, the current density equals j_s/β_i. For spherical coordinates, the condition for source limited current is $j_e\beta_i^2 > j_s$ and the corresponding emission surface current density is j_s/β_i^2.

In conclusion, the finite element approach gives improved accuracy for numerical modeling of charged particle guns. The main difficulty is dealing with arbitrary mesh geometries. The problem is challenging for space-charge-limited emission, where there is a singularity at the particle source. The emission surface procedure described in this paper resolves the problem for sources of arbitrary shape. To model space charge in the region between the source and emission surface, the method applies the same techniques used for particle tracking and space-charge assignment in downstream regions. Good approximations for the space charge and potential variations can be derived by tracking particles backward from the emission surface to the source at a specific constant velocity. The method is easily extended to accommodate multiple emission regions, sharply curved sources, and mixed source-limited and space-charge-limited emission.

ACKNOWLEDGMENTS

This work was partially supported by North Star Research Corporation through Department of Energy SBIR Grant Number DE-FG05-91ER81209. I thank Richard Adler for his suggestions and encouragement. I am also grateful to the Accelerator Code Group of Los Alamos National Laboratory for permission to use finite-element routines from the Lattice and Poisson programs originally developed by Ronald Holsinger.

REFERENCES

1. See, for instance, W. Scharf, *Particle Accelerators and Their Uses* (Harwood Academic, Chur, Switzerland, 1986).
2. See, for instance, S. Humphries Jr., *Charged Particle Beams* (Wiley, New York, 1990), Section 7.3.
3. W. B. Herrmannsfeldt, Stanford Linear Acc. Center, SLAC-331, 1988 (unpublished).
4. A. C. Paul, Lawrence Berkeley Lab, LBL-13241, 1982 (unpublished).
5. D. L. Vogel, Lawrence Berkeley Lab., LBL-18871, 1985 (unpublished).
6. J. E. Boers, Sandia National Labs, SAND 79-1027, 1980 (unpublished).
7. R. True, *IEEE Trans. Nucl. Sci.* **NS-32,** 2611 (1985); "General Purpose Relativistic Beam Dynamics Code," in *Computational Accelerator Physics,* edited by R. Ryne (Am. Inst. of Phys., New York, 1994), p. 493.
8. S. Humphries Jr., "TRAK," in *Computational Accelerator Physics*, edited by R. Ryne (Am. Inst. of Phys., New York, 1994), p. 597; "Integrated Software System for High-power Beam Design," in *Beams 94: Proceedings, 10th Conf. High Power Particle Beams* (National Technical Information Service, NTIS PB95-144317, 1995), p. 568.
9. A. M. Winslow, *J. Comput. Phys.* **1**(2), 149 (1967).
10. Accelerator Code Group, Los Alamos National Laboratory, LA-UR-87-126, 1987, Section B.13.6.2 (unpublished).
11. See, for instance, M. N. O. Sadiku, *Numerical Techniques in Electromagnetics* (CRC Press, Boca Raton, FL, 1992), Chap. 6.
12. See, for instance, W. H. Press, S. A. Teukolsky, W. T. Vetterling, and B. P. Flannery, *Numerical Recipes in Fortran*, 2nd ed. (Cambridge Univ. Press, Cambridge, 1992), Section 16.1.
13. S. Humphries Jr., [2, Section 5.2].
14. C. D. Child, *Phys. Rev.* **32,** 492 (1911).
15. D. Potter, *Computational Physics* (Wiley, New York, 1973), p. 88.
16. J. R. Pierce, *Theory and Design of Electron Beams* (Van Nostrand, Princeton, NJ, 1949).
17. Registered trademark of Intel Corporation.
18. I. Langmuir and D. Blodgett, *Phys. Rev.* **24,** 49 (1924).
19. W. H. Press, S. A. Teukolsky, W. T. Vetterling, and B. P. Flannery, [12, Section 17.1].